PHYSICAL REVIEW B VOLUME 26, NUMBER 9 1 NOVEMBER 1982

Monte Carlo simulations of one-dimensional fermion systems

J. E. Hirsch and R. L. Sugar
Institute for Theoretical Physics, University of California, Santa Barbara, California 93106

D. J. Scalapino
Department of Physics and Institute for Theoretical Physics, University of California, Santa Barbara, California 93106

R. Blankenbecler
Stanford Linear Accelerator Center, Stanford University, Stanford, California 94305
(Received 27 May 1982)

We discuss a new method to perform numerical simulations of one-dimensional systems with fermion and boson degrees of freedom. The method is based on a direct-space, imaginary-time representation of the fermion field. It is fast so that systems having up to 100 sites can easily be simulated. In addition, the method provides an intuitive physical "picture" of the ground state of a one-dimensional many-body system. We discuss in detail how to implement the method and how to compute various physical quantities. In particular, we show how to extend the method to study averages of off-diagonal quantities in an occupation-number representation. To assess the accuracy of our procedure, we apply it to free fermions in one dimension and compare with exact results. We then study a model of spinless interacting fermions and obtain the expected phase structure and behavior of correlation functions. We also consider the extended Hubbard model at various points in its phase diagram and study the behavior of spin-density, charge-density, and pairing correlation functions. We then study the Gross-Neveu model and show how the behavior depends on the number of fermion flavors. Finally, we consider an electron-phonon model and study its behavior both in the one-particle polaron sector and in the half-filled-band case. Along the way we show pictures of the ground-state configurations that give physical insight into the properties of the systems, like charge-density-wave, spin-density-wave, and superconducting states, "fractional charges," and solitons. We conclude by comparing our method with other methods and discuss the possibility of extending it to higher dimensions.

I. INTRODUCTION

Numerical simulation represents an important new technique for exploring the physical properties of interacting quantum fields. On a qualitative level it allows one to determine whether a particular model exhibits the essential physical characteristics one is seeking and to develop a feeling for the way in which the parameters of the model affect its physical behavior. One can try a variety of "*gedanken*" experiments to obtain new insights as well as explore the feasibility of various possible real experiments. On another level, detailed simulations allow one to obtain quantitative data on properties of complex systems which can then be compared with actual measurements, exact solutions in special cases, or approximate analytic calculations.

The route to simulating quantum fields proceeds via Feynman's path-integral representation. As Feynman showed, the quantum-mechanical properties of a particle can be obtained by summing an exponential of the action over classical paths.[1] The simulation of these paths involve only real variables and can therefore be easily programmed.[2] This has a direct generalization for boson fields. However, for fermion fields, the anticommuting nature of the field operators, reflecting the Pauli principle, leads to paths that are parametrized by noncommuting c-number fields which so far have not lent themselves to direct numerical evaluation.

The canonical way in which fermion-field theories have been treated is by considering (or by constructing with the aid of auxiliary boson fields) models which are bilinear in the fermion fields. Then the path integrals over the fermion fields are formally carried out yielding a determinant which depends upon the boson fields. The problem is thus reduced to a boson path integral with an effective action which depends upon the determinant of a very large matrix. Various approaches to reducing

the time required to evaluate such determinants have been proposed.[3]

Here, however, we will focus on an alternative method which has proven useful for treating fermion fields in one space and one time dimension.[4] In this approach we work with the canonical ensemble, so the average value of a physical observable, A, is given by

$$\langle A \rangle = \mathrm{tr} \frac{(Ae^{-\beta H})}{\mathrm{tr}(e^{-\beta H})} . \tag{1.1}$$

Here H is the Hamiltonian of the system and β is the inverse temperature. Since the fermion number is fixed, one can consider a single fermion up to a many-fermion system. We will often work with a half-filled band in both condensed-matter and relativistic-field-theory applications.

In order to evaluate the traces in Eq. (1.1) we break up the imaginary-time interval $0 \leq \tau \leq \beta$ into small slices and introduce complete sets of states at each time slice. The many sums over intermediate fermion states are then carried out by importance sampling techniques. This procedure will be shown to be extremely fast. The computer time required is similar to that for a Monte Carlo (MC) simulation of the classical two-dimensional Ising model. It is possible to treat interacting fermion fields without the necessity of introducing auxilliary boson fields, further speeding up the calculation in comparison to other methods. Furthermore, the sum over states has a natural graphical representation which can provide useful insight into the nature of the state of an interacting many-fermion system.

In carrying out the numerical simulations we introduce a finite spatial lattice and work at a finite value of β. We generally use periodic spatial boundary conditions, although we have run simulations with both antiperiodic and open boundary conditions. For certain ring molecules, a finite lattice may be the more appropriate physical description; however, if the infinite chain or continuum limit is of interest one must extrapolate the finite-lattice results. Lattices containing as many as 100 sites have been treated without difficulty. Similarly, if the ground-state properties of a system are of interest one must extrapolate to values of β^{-1} which are smaller than the other energy scales in the problem. In some cases this simply involves taking a lattice which is large compared to the range of spatial or imaginary-time correlations. In other cases associated with phase transitions in the ground state, it may be necessary to use some type of finite-size scaling procedure.

We have previously given a brief description of our method.[4] Here we present a detailed discussion of the technique along with results for a variety of different models. In Sec. II we formulate the method, discuss the graphical representation of the paths, and show how to compute physical quantities. In Secs. III–VI we present a number of results which we have obtained using the simulation techniques described in Sec. II. To illustrate the range of problems which can be treated with this approach, we consider a number of different models and a variety of measurements ranging in character from quantitative to qualitative.

In Sec. III we begin by studying a model of spinless fermions with nearest-neighbor interactions described by the Hamiltonian

$$H = -t \sum_i (C_i^\dagger C_{i+1} + C_{i+1}^\dagger C_i) + V \sum_i (n_i - \tfrac{1}{2})(n_{i+1} - \tfrac{1}{2}) . \tag{1.2}$$

Here $C_i^\dagger$ and C_i are the creation and annihilation operators for a fermion at the ith spatial lattice site, and $n_i = C_i^\dagger C_i$. This simple model has a nontrivial phase structure; with a half-filled band and $0 \leq V/2t \leq 1$ the charge-density correlation function $\langle n_i n_{i+l} \rangle$ decays algebraically with l and there is no long-range order or gap in the spectrum of the infinite, zero-temperature system. However, for $V/2t > 1$, the ground state has a charge-density wave, (CDW) and the space and time correlations are characterized by a correlation length and gap, respectively. As $V/2t \to 1+$ the order parameter, the inverse correlation length and the gap all vanish with an essential singularity.

In Sec. IV we study the extended Hubbard model. This model can be obtained from that of Eq. (1.2) by allowing the fermions to have spin and by including an onsite interaction $U \sum n_{i\uparrow} n_{i\downarrow}$. This model is known to have a rich ground-state phase diagram in the U-V parameter space consisting of charge-density, spin-density, and singlet- and triplet-pairing phases. We will examine typical path configurations and correlation functions to obtain a qualitative feeling for these different regimes.

When $V > 0$ and $U = -2V$, one is in the charge-density-wave sector. This particular line in the parameter space of the extended Hubbard model corresponds to the Gross-Neveu model with two flavors ($N_f = 2$). We have also simulated the Gross-Neveu model itself with up to ten flavors and in Sec. V some results are compared with analytic expressions using an N_f^{-1} expansion.

There are also a variety of interesting problems

which involve coupled fermion-boson fields. These range from condensed-matter models of electron-phonon systems to relativistic gauge models such as the Schwinger model.[5] In these systems the retarded nature of the interaction between the fermions which is mediated by the bosons can be important and one seeks to treat both fields on an equal footing. In Sec. VI we illustrate some features of our method as applied to problems of this type by considering the one-dimensional electron-phonon Hamiltonian

$$H=-t\sum(C_{i+1}^{\dagger}C_i+C_i^{\dagger}C_{i+1}) +\tfrac{1}{2}\sum\left[\frac{p_i^2}{M}+Kx_i^2\right]\lambda\sum x_i(n_i-\tfrac{1}{2}) . \quad (1.3)$$

Here harmonic oscillators representing local molecular distortions on each site are coupled to the electron charge on the site while the electrons can hop from one site to the next via the transfer matrix element t. If an electron occupies a site, the molecule tends to distort, making x_i negative if $\lambda>0$. In the one-fermion sector, this model describes a polaron.[6] For a half-filled band, there is a tendency to have an alternating molecular distortion which can open up a band gap in the fermion spectrum. This Peierls[7] state is the ground state in the adiabatic limit when the oscillator mass $M\to\infty$. However, as M decreases, the zero-point motion of the oscillators can wash out this behavior and cause the gap to vanish. In Sec. VI various properties of this system will be discussed. In Sec. VII we conclude with a comparison of this technique with other methods[8] and a discussion of the problems associated with extending it to higher dimensions.

II. THE MONTE CARLO PROCEDURE

In this section we develop the formalism we have employed for carrying out Monte Carlo calculations of one-dimensional systems with fermion degrees of freedom.

A. Formalism

We work with the canonical ensemble, so the average value of a physical observable is given by Eq. (1.1). For systems with boson degrees of freedom the standard procedure for carrying out numerical simulations makes use of the path-integral expressions for the traces of Eq. (1.1). For systems with fermion degrees of freedom we wish to develop a formalism that does not involve the anitcommuting c-number fields of the ordinary fermion path integrals.

As in the standard derivation of the path integrals, we begin by dividing the imaginary-time interval $0<\tau<\beta$ into L subintervals of width $\Delta\tau=\beta/L$. At each time slice we insert a complete set of states so that the partition function, for example, is given by

$$Z=\mathrm{tr}\,(e^{-\beta H}) =\sum_{i_1,\ldots,i_L}\langle i_1|e^{-\Delta\tau H}|i_L\rangle\langle i_L|e^{-\Delta\tau H}|i_{L-1}\rangle\cdots \times\langle i_2|e^{-\Delta\tau H}|i_1\rangle . \quad (2.1)$$

In general the matrix elements in Eq. (2.1) will not be easy to evaluate. However, it is usually possible to write the Hamiltonian in the form

$$H=H_1+H_2 , \quad (2.2)$$

with H_1 and H_2 each being trivially diagonalizable. Then with the use of the fact[9] that for small $\Delta\tau$,

$$e^{-\Delta\tau H}=e^{-\Delta\tau H_2}e^{-\Delta\tau H_1}[1+O(\Delta\tau^2)] , \quad (2.3)$$

and inserting additional intermediate states we have

$$Z=\sum_{i_1,\ldots,i_{2L}}\langle i_1|U_1|i_{2L}\rangle\langle i_{2L}|U_2|i_{2L-1}\rangle \times\langle i_{2L-1}|U_1|i_{2L-2}\rangle\cdots\langle i_2|U_2|i_1\rangle , \quad (2.4)$$

where

$$U_i=e^{-\Delta\tau H_i} .$$

Then by a judicious choice of the complete sets of intermediate states, all the matrix elements in Eq. (2.4) can be directly evaluated. This general approach was first proposed by Suzuki *et al.*[10]

Let us first recall how this works for a system with bosonic degrees of freedom. If we denote by x_i the field coordinate on the ith lattice site and by p_i the momentum conjugate to x_i, then the Hamiltonian can ordinarily be written in the form

$$H=\tfrac{1}{2}\sum_{i=1}^{N}p_i^2+V(x_1,\ldots,x_N) . \quad (2.5)$$

We take

$$H_1=\tfrac{1}{2}\sum_{i=1}^{N}p_i^2 \text{ and } H_2=V , \quad (2.6)$$

and then choose $|i_j\rangle$ to be eigenstates of the momentum operators for j odd and eigenstates of the coordinate operators for j even; thus all the matrix elements in Eq. (2.4) can be evaluated immediately. Since the Hamiltonians is quadratic in the momentum operators, the sums over momentum eigenstates can also be carried out, and letting $\Delta\tau\rightarrow 0$ we obtain the standard path-integral expression for the partition function

$$Z=\int \delta x\, e^{-S}, \tag{2.7}$$

with

$$S=\int_0^\beta d\tau\left[\frac{1}{2}\sum_{i=1}^{N}\left(\frac{\partial x_i(\tau)}{\partial\tau}\right)^2 + V(x_1(\tau),\ldots,x_N(\tau))\right]. \tag{2.8}$$

For systems with fermions we use a different breakup. In this paper we shall consider models with nearest-neighbor hopping and interactions among the fermions such as those of Eqs. (1.2) and (1.3). It is possible to extend the following discussion to include non-nearest-neighbor-hopping terms and long-range interactions.

Let us start by considering systems without boson degrees of freedom. The Hamiltonian can be written in the form

$$H=\sum_{i=1}^{N} H_{i,i+1}, \tag{2.9}$$

where $H_{i,i+1}$ contains only fermion creation and annihilation operators for sites i and $i+1$. Using periodic boundary conditions implies $H_{N,N+1}\equiv H_{N,1}$. We now choose[11,12]

$$H_1=\sum_{i\ \text{odd}} H_{i,i+1},\qquad H_2=\sum_{i\ \text{even}} H_{i,i+1}. \tag{2.10}$$

Notice that H_1 and H_2 are each composed of a sum of $N/2$ mutually commuting terms. So, for example,

$$U_1=e^{-\Delta\tau H_1}=\prod_{i\ \text{odd}} e^{-\Delta\tau H_{i,i+1}}. \tag{2.11}$$

As a result, to compute the matrix elements of Eq. (2.4) we need only solve a two-site problem which has a small number of degrees of freedom.

As an example, consider the model of Eq. (1.2),

$$H_{i,i+1}=-t\sum(C_{i+1}^\dagger C_i+C_i^\dagger C_{i+1}) + V(n_i-\tfrac{1}{2})(n_{i+1}-\tfrac{1}{2}). \tag{2.12}$$

If we denote by $|n_i n_{i+1}\rangle$ the state in which there are n_i fermions on the ith lattice site and n_{i+1} on the $(i+1)$th $(n_i,n_{i+1}=0,1)$, then it is easy to see that

$$\begin{aligned} e^{-\Delta\tau H_{i,i+1}}|0,0\rangle &= |0,0\rangle e^{-\Delta\tau V/4},\\ e^{-\Delta\tau H_{i,i+1}}|1,1\rangle &= |1,1\rangle e^{-\Delta\tau V/4},\\ e^{-\Delta\tau H_{i,i+1}}|1,0\rangle &= [\cosh(\Delta\tau t)|1,0\rangle + \sinh(\Delta\tau t)|0,1\rangle]e^{\Delta\tau V/4},\\ e^{-\Delta\tau H_{i,i+1}}|0,1\rangle &= [\cosh(\Delta\tau t)|0,1\rangle + \sinh(\Delta\tau t)|1,0\rangle]e^{\Delta\tau V/4}. \end{aligned} \tag{2.13}$$

For $V=0$, Eq. (2.13) has a simple interpretation. A single fermion moves forward with matrix element $\cosh(\Delta\tau t)$ or hops one site to the left or right with matrix element $\sinh(\Delta\tau t)$. We may think of two fermions on adjacent sites as moving forward with matrix element $\cosh(\Delta\tau t)^2$ and interchanging by hopping past each other with matrix element $-\sinh(\Delta\tau t)^2$. Note that our procedure groups these two possibilities together giving a weight of 1. Thus our method always gives positive weights in one dimension in contrast to the approach of Ref. 12.

B. Thermalization

Within each time interval $\Delta\tau$ there is one application of the operator U_1 and one of the operator U_2. This leads to the graphical representation shown in Fig. 1. Here the periodic spatial lattice of sites is labeled by n and the imaginary-time axis τ has been sliced into $2\beta/\Delta\tau$ segments. The occupation on each τ slice corresponds to one of the states $|i_k\rangle$ in the sum for Z, Eq. (2.4). The shaded boxes correspond to the areas of space and imaginary time in which fermions can hop and interact. The sum over intermediate states in Eq. (2.4) corresponds to the sum over all possible ways of distributing the fermions on the spatial lattice at each time slice.

In performing the sum over fermion configurations by importance sampling, we randomly generate new configurations and accept or reject them according to an alogrithm, such as the heat-bath al-

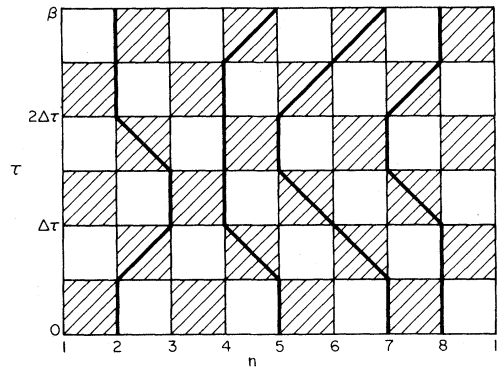

FIG. 1. Breakup of the time-evolution operator given by Eqs. (2.3) and (2.10) leads to the checkerboard pattern shown in this figure. Fermions can hop and interact in the shaded square but not in the unshaded ones. Heavy lines are examples of allowed fermion world lines.

gorithm, which ensures that the probability of a configuration being sampled is proportional to the product of matrix elements in Eq. (2.4). In generating new configurations, we want to take into account the conservation laws associated with the Hamiltonian, otherwise a large amount of computer time will be wasted generating configurations that have zero probability of being accepted.

Fermion number is always conserved, and with our breakup procedure it is conserved by each $H_{i,i+1}$, that is within each shaded box in Fig. 1. In Fig. 1 the occupied sites at each τ slice have been connected by lines which we will call the world lines of the fermions. The sum over intermediate states that satisfy fermion-number conservation is equivalent to the sum over all allowed configurations of the world lines. Notice that *world lines* can be drawn along the vertical edge of a shaded box or diagonally across a shaded box, but they *cannot be drawn diagonally across an unshaded box.*

This graphical representation gives a simple picture of a particular path configuration which enters Eq. (2.1). These configurations also can provide insight into the state of the many-fermion system. Consider the partition function traced over energy eigenstates $|\psi_\alpha\rangle$,

$$Z=\sum_\alpha \langle \psi_\alpha | e^{-\beta H} | \psi_\alpha \rangle . \tag{2.14}$$

Now separate $e^{-\beta H}$ into $e^{-(\beta-\tau)H}e^{-\tau H}$ and insert a complete set of occupation-number states between the two exponentials. In the limit of low temperatures, only the ground state $|\psi_0\rangle$ contributes and for each τ slice we have

$$Z=e^{-\beta E_0}\sum_{\{n_i\}} |\langle n_1,\ldots,n_N | \psi_0 \rangle|^2 . \tag{2.15}$$

Thus for any time slice the probability of having a given set of occupation numbers $|n_1,\ldots,n_N\rangle$ is proportional to the square of the projection of the ground state on $|n_1,\ldots,n_N\rangle$. In this way, a path configuration taken for large β can provide a picture of the ground state of a many-fermion system.

We wish to develop an algorithm for generating all allowed world-line configurations. In the Monte Carlo simulation of boson-field theories, one builds up general field configurations by making successive local changes in the fields. We want to do the same with the world lines. We cannot move a fermion at a single site since if we start from an allowed configuration that would always lead to fermion nonconservation in at least one shaded box. The minimum change we can make is to move two fermions from one vertical edge of an unshaded box to the other as is illustrated in Fig. 2. By making successive moves of this type we can generate all world-line configurations of a given winding number.

We define the winding number of a configuration in the following manner. Because we are evaluating a trace and using periodic boundary conditions, Fig. 1 has the topology of a torus. Suppose we start at any occupied site at time $\tau=0$ and follow a world line continuously through one revolution (τ increases from 0 to β and returns to 0). If we arrive back at the same spatial site after one revolution, we say the configuration has a winding number of 0. If we require n revolutions to return to the same spatial site, we say that the configuration has a winding number of $\pm(n-1)$ depending on whether we move in the positive or negative spatial direction with each revolution. In most applications[13] for all

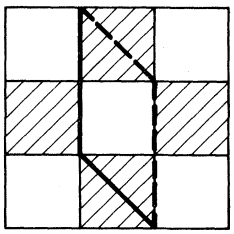

FIG. 2. Example of an allowed local change in a fermion world line. The world line can move from one vertical edge of an unshaded box to the other. Solid line shows the world line before the move and the dashed line after the move.

but the smallest spatial lattices (i.e., $N \geq 6$) only configurations with a winding number of 0 are important as we have verified by direct calculation. Configurations with winding numbers greater than 0 only arise when periodic boundary conditions are imposed and do not occur, for example, with fixed-end boundary conditions. We do not include them in the Monte Carlo calculations discussed here, although it is possible to do so by modifying the initial conditions.

We are now in a position to present the details of our Monte Carlo algorithm. For definiteness we consider the model of Eq. (1.2). We designate each lattice point by (i,j), where i gives the spatial and j the temporal position, $i=1,\ldots,N$ and $j=1,\ldots,2L$. At each lattice site, we define an occupation number $n(i,j)$ which is 0 if the site is unoccupied and 1 if it is occupied. In sweeping through the lattice, we must check whether it is possible to move a world line across each unshaded square. Let us focus on the unshaded square whose lower left-hand corner is at the site (i,j). A move is possible across this square if and only if $s=\pm 2$, where

$$s \equiv n(i,j)+n(i,j+1)-n(i+1,j) \\ -n(i+1,j+1) . \tag{2.16}$$

A plus sign will allow a move from left to right and the minus sign from right to left. If a move is possible, we must calculate the ratio of the product of matrix elements in Eq. (2.4) after and before the move. Denote this ratio by R. R will depend on the occupation numbers $n(i+1,j-1)$ and $n(i+1,j+2)$ because they determine whether the world line we are moving is vertical or diagonal in the shaded boxes above and below our unshaded one. R will also depend on $n(i-1,j)$ and $n(i+2,j)$ because they determine whether there is an additional world line running through the shaded boxes to the left and right of our unshaded one. Referring to Eq. (2.13), we see that

$$R=[\tanh(\Delta\tau t)]^{su}[\cosh(\Delta\tau t)]^{sv}e^{\Delta\tau V s v/2} , \tag{2.17}$$

where

$$u=1-n(i+1,j-1)-n(i+1,j+2) , \\ v=n(i-1,j)-n(i+2,j) , \tag{2.18}$$

and s is defined in Eq. (2.16).

Since we are only considering two possible configurations of the world line under study, we use the heat-bath algorithm for accepting or rejecting new configurations. That is, we accept the proposed new configuration with probability

$$P=\frac{R}{(1+R)} . \tag{2.19}$$

This completes our description of the Monte Carlo algorithm for the model of Eq. (1.2). The assertion made in the introduction that it is as fast as the usual algorithm for the classical two-dimensional Ising model should now be obvious.

C. Measurements

Once the system has been brought into statistical equilibrium, we can make measurements of physically interesting quantities. There are two classes of operators for which the averaging procedure has to be done in a somewhat different way, which we now discuss.

1. Operators that conserve fermion number locally

The computation of averages for this type of operator proceeds in essentially the same manner as in a Monte Carlo simulation of a classical system. Referring back to Eq. (2.4), the intermediate state $|i_j\rangle$ specifies the distribution of fermions in the jth intermediate state. The Monte Carlo algorithm generates a sequence of distributions $i_1(k),\ldots,i_{2L}(k)$, $k=1,2,\ldots,M$, such that the probability of a particular distribution, k, is given by

$$P(k)=\frac{\langle i_1(k)|U_1|i_2(k)\rangle\langle i_2(k)|U_2|i_3(k)\rangle\cdots\langle i_{2L}(k)|U_2|i_1(k)\rangle}{\sum_{i_1,\ldots,i_{2L}}\langle i_1|U_1|i_2\rangle\langle i_2|U_2|i_3\rangle\cdots\langle i_{2L}|U_2|i_1\rangle} . \tag{2.20}$$

Consider first operators that are diagonal in the occupation-number representation. Examples of this type are the staggered order parameter

$$Q=\sum_{i=1}^{N}(-1)^i n_i , \tag{2.21}$$

and the density-density correlation function

$$G(i-j,\tau)=\langle n_i(\tau)n_j(0)\rangle , \tag{2.22}$$

where

$$n_i(\tau)=e^{\tau H}n_i e^{-\tau H} . \tag{2.23}$$

We have, for example,

$$\langle Q\rangle=\lim_{M\to\infty}\frac{1}{2LM}\sum_{k=1}^{M}\sum_{j=1}^{2L}\sum_{i=1}^{N}(-1)^{i}n_k(i,j)\ , \tag{2.24}$$

where $n_k(i,j)$ is the value of $n(i,j)$ in the kth configuration sampled, and M is the total number of configurations sampled.

A very similar procedure applies to operators that, without being diagonal in the occupation-number representation, conserve number of particles within a two-site block. Examples of these are the average energy

$$E=-\frac{\partial}{\partial\beta}\ln Z=\langle H\rangle\ , \tag{2.25}$$

the specific heat

$$C=\frac{\partial E}{\partial T}\ , \tag{2.26}$$

and the current-current correlation function

$$C(\tau)=\langle j(\tau)j(0)\rangle\ , \tag{2.27}$$

with

$$j=i\sum_i(C_i^\dagger C_{i+1}-C_{i+1}^\dagger C_i) \tag{2.28}$$

and the time dependence given by Eq. (2.23). For simplicity, consider the average of an operator A,

$$\langle A\rangle=\mathrm{tr}[A(U_1U_2)^L]/Z\ , \tag{2.29}$$

where A is such that it allows an identical decomposition as the Hamiltonian [Eq. (2.10)], $A=A_1+A_2$. We can then write

$$\langle A\rangle=\mathrm{tr}\left[P(i_1,\ldots,i_{2L})\left[\frac{\langle i_1|A_1U_1|i_2\rangle}{\langle i_1|U_1|i_2\rangle}+\frac{\langle i_{2L}|U_2A_2|i_1\rangle}{\langle i_{2L}|U_2|i_1\rangle}\right]\right] \tag{2.30}$$

to order $(\Delta\tau)^2$. We have then simply to compute the matrix elements given in Eq. (2.30) for each box configuration and the averaging proceeds in the usual way. As an example, consider the average energy for the model, Eq. (1.2). For shaded boxes with no or two fermions, we just obtain a contribution to the average energy of $V/4$. For boxes with a single fermion moving forward, the contribution is

$$-\left[t\tanh(\Delta\tau t)+\frac{V}{4}\right]\ ,$$

while for a single fermion moving diagonally the contribution is

$$-\left[t\coth(\Delta\tau t)+\frac{V}{4}\right]\ .$$

2. *Operators that do not conserve fermion number locally*

The evaluation of averages for this type of operator is somewhat more complicated. Examples are the single-particle Green's function

$$g(k-j,\tau)=\langle C_k(\tau)C_j^\dagger(0)\rangle\ , \tag{2.31}$$

and the singlet-pairing correlation function,

$$D(i-j,\tau)=\langle C_{i\uparrow}^\dagger(\tau)C_{i\downarrow}^\dagger(\tau)C_{j\uparrow}(0)C_{j\downarrow}(0)\rangle\ , \tag{2.32}$$

which measures superconductivity correlations and is therefore of great interest. Consider for definiteness the equal-time single-particle Green's function

$$g(k-j)=\langle C_k^\dagger C_j\rangle=\frac{\mathrm{tr}[C_k^\dagger C_j(U_1U_2)^L]}{\mathrm{tr}[(U_1U_2)^L]}\ . \tag{2.33}$$

If we try to use a procedure like that given in Eq. (2.30),

$$g(k-j)=\mathrm{tr}\left[\frac{\langle i_1|C_k^\dagger C_jU_1|i_2\rangle}{\langle i_1|U_1|i_2\rangle}P(i_1,\ldots,i_{2L})\right]\ , \tag{2.34}$$

and it becomes immediately clear that Eq. (2.34) is not well defined.

The reason is that for $|k-j|>1$ there exist configurations where the numerator in Eq. (2.34) is nonzero but the denominator is zero. For example, a configuration where state $|i_1\rangle$ has a world line terminating at site k and state $|i_2\rangle$ has one starting at site j.

To get around this problem, we insert an additional intermediate state and write

$$g(k-j)=\frac{\mathrm{tr}(\langle i_1|C_k^\dagger C_j|i_1'\rangle\langle i_1'|U_1|i_2\rangle\cdots\langle i_{2L}|U_2|i_1\rangle)}{\mathrm{tr}(\langle i_1|i_1'\rangle\langle i_1'|U_1|i_2\rangle\cdots\langle i_{2L}|U_2|i_1\rangle}\equiv\frac{\ll i_1|C_k^\dagger C_j|i_1'\gg_{\tilde P}}{\ll i_1|i_1'\gg_{\tilde P}}\ , \tag{2.35}$$

where the averages are now with respect to the probability

$$\tilde{P}=\frac{\langle i_1' \mid U_1 \mid i_2\rangle \cdots \langle i_{2L} \mid U_2 \mid i_1\rangle}{\sum_{i_1', i_1, \ldots, i_{2L}} \langle i_1' \mid U_1 \mid i_2\rangle \cdots \langle i_{2L} \mid U_2 \mid i_1\rangle} . \tag{2.36}$$

Note that there is no time-evolution operator in $\tilde{P}$ connecting states $|i_1\rangle$ and $|i_1'\rangle$. The world lines are now allowed to be "disconnected" across these states. The Monte Carlo sweeps are done with the Boltzmann weight $\tilde{P}$. An example of an allowed configuration is shown in Fig. 3. In practice, we only allow for at most one world line to be disconnected for computing single-particle Green's functions. (It is easy to convince oneself that this restriction is valid.) Each time that the states $|i_1\rangle$ and $|i_1'\rangle$ coincide, we get a contribution to the denominator in Eq. (2.35), and when they satisfy

$$|i_1\rangle = \pm C_k^\dagger C_j |i_1'\rangle ,$$

we get a contribution to the numerator. The statistics are somewhat worse than for the other kinds of averages, since we make measurements at only one time slice. In addition, the quantity of interest involves now the *ratio* of two averages.

A similar procedure applies for time-displaced correlation functions of this type. For the correlation function (2.31), for example, we have to insert two additional intermediate states, one at time 0 and one at time τ. In addition, we have to perform *two* Monte Carlo simulations for the time interval $0<\tau'<\tau$, one in which there is an extra fermion in that interval and one in which there is not. The latter is needed to calculate the normalization integral.

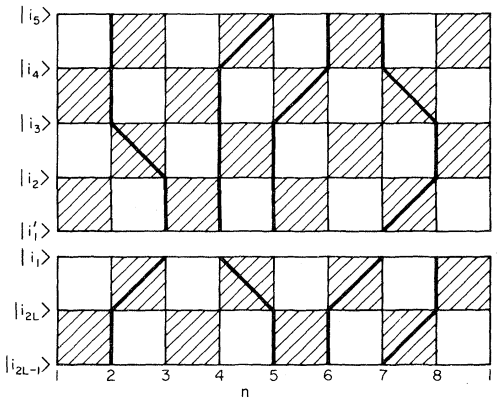

FIG. 3. Allowed world-line configuration for the calculation of the equal-time single-particle correlation function. World lines do not need to be connected between the states $|i_1\rangle$ and $|i_1'\rangle$.

The final generalization discussed here is to include boson degrees of freedom as in the Hamiltonian of Eq. (1.3). We simply extend the Hilbert space of the intermediate states and proceed in the standard way. We obtain the usual functional integral over the boson coordinates and treat the sum over fermion states in the manner just described. In carrying out the Monte Carlo calculation, the change in matrix elements due to the movement of a fermion world line will, of course, depend on the boson-field configuration, and the change due to a local variation in the boson field will depend on the fermion distribution.

We conclude this section by estimating the error made in the breakup of the time-evolution operator, $\exp(-\Delta\tau H)$, defined by Eqs. (2.3), (2.9), and (2.10). Now we know that the Hamiltonian, H, has eigenvalues that grow linearly with N. Since $\Delta\tau=\beta/L$, for $L\approx N$, the operator $\Delta\tau H$ has matrix elements of order β, so for large β, a series expansion of the exponential is not expected to be useful. On the other hand, in Eq. (2.3) the error is proportional to commutators of H_1 and H_2 rather than powers of H. We have tested our breakup procedure by studying free-field theory. In particular, we consider the Hamiltonian of Eq. (1.2) with $V=0$, $t=1$, and a half-filled band. In Tables I and II we compare results for the average energy and specific heat obtained with our breakup procedure to the exact values and to the results obtained by expanding $\exp(-\Delta\tau H)$ to first and second order in $\Delta\tau H$.

III. INTERACTING SPINLESS FERMIONS

To begin, consider a single spinless fermion hopping on a one-dimensional lattice,

$$H=-t\sum_i (C_{i+1}^\dagger C_i + \text{H.c.}) . \tag{3.1}$$

We start the system in the configuration shown in Fig. 4(a). Here there are 48 lattice sites, and a "1" is printed if an electron occupies a site. Carrying out the Monte Carlo procedure discussed in Sec. II we obtain, after warming up the system, typical paths like the one shown in Fig. 4(b). The single-particle eigenstates of Eq. (3.1) on a lattice of N (even) sites have energies $\epsilon_k=-2t\cos k$ with $k=2\pi n/N$ ($n=0,\pm1,\ldots,+N/2$). If $t\gg kT$, then only the low-lying states are occupied so that over the energy range of importance $\epsilon_k\simeq -2t+tk^2$, and the particles behave as if they were free with a mass

TABLE I. Internal energy per site for free fermions. [The model of Eq. (1.2) with $t=1$ and $V=0$]. N is the number of lattice sites and $N/2$ the number of fermions. E is the exact results and E_{CB} the result from the checkerboard breakup of Eqs. (2.3) and (2.10). E_1 and E_2 are obtained from expanding $e^{-\Delta\tau H}$ to first and second order in $\Delta\tau$. In this example $L=N$ and $\Delta\tau=0.1$.

N	E	E_{CB}	E_1	E_2
4	−0.242	−0.242	−0.152	−0.234
8	−0.388	−0.389	−0.301	−0.382
16	−0.539	−0.540	−0.454	−0.532
24	−0.593	−0.594	−0.508	−0.586

TABLE II. Specific heat for free fermions [the model of Eq. (1.2) with $t=1$ and $V=0$]. N is the number of lattice sites, and $N/2$ the number of fermions. C is the exact result and C_{CB} the result from the checkerboard breakup of Eqs. (2.3) and (2.10). C_1 and C_2 are obtained from expanding $e^{-\Delta\tau H}$ to first and second order in $\Delta\tau$. In this sample $L=N$ and $\Delta\tau=0.1$.

N	C	C_{CB}	C_1	C_2
4	0.32	0.32	0.20	0.25
8	1.74	1.76	1.30	1.57
16	4.94	5.00	3.09	5.49
24	5.92	6.04	1.67	454.00

$m=1/(2t)$. For free particles, the continuum correlation function for a time separation τ varies as

$$\langle n(j,\tau)n(i,0)\rangle \propto e^{-(m/\tau)|x_i-x_j|^2} . \tag{3.2}$$

On a discrete time lattice, the continuum behavior will be approached when $\tau \gg \Delta\tau$ and, because of the periodic boundary conditions, when $(\beta-\tau)\gg\Delta\tau$. Thus we choose $\tau=\beta/2$ and normalize Eq. (3.2),

$$C(j-i)=\frac{\langle n(j,\beta/2)n(i,0)\rangle}{\langle n(i,\beta/2)n(i,0)\rangle} , \tag{3.3}$$

so that in the continuum limit,

$$\sqrt{-\ln[C(j-i)]}=\left[\frac{2m}{\beta}\right]^{1/2}|x_j-x_i| . \tag{3.4}$$

Figure 5 shows the results obtained by averaging over 1000 configurations with $t=1$ and $\beta=2.25$. The dashed line corresponds to the continuum limit given by Eq. (3.4), while the solid line corresponds to the result using the actual-band eigenstates. The points are the Monte Carlo data. This illustrates that the trajectory shown in Fig. 4(b) does in fact correspond to an x-space picture of a single-electron state. Figure 6 shows the same system with eight electrons moving without interactions, but of course obeying the Pauli principle.

As discussed in the Introduction, the half-filled band with a near-neighbor Coulomb interaction V is of particular interest since there is a phase transition to a charge-density-wave ground state when

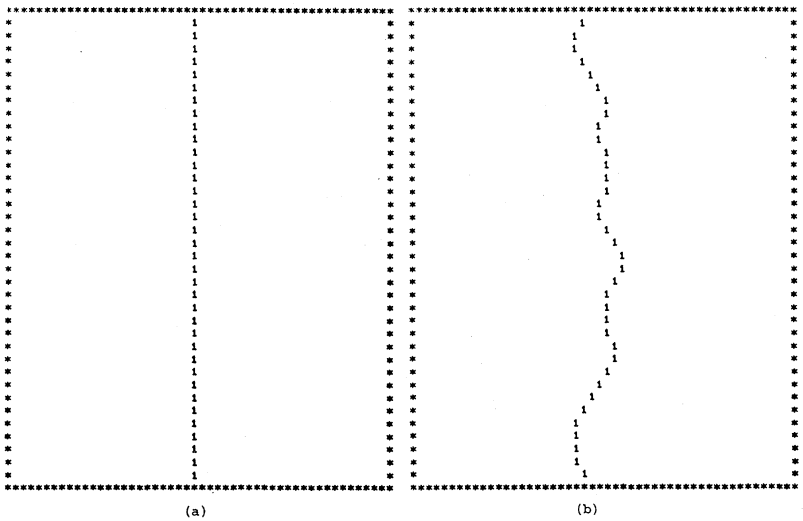

FIG. 4. (a) Initial configuration of one fermion on a 48-site lattice with 18 time slices with $\Delta\tau=0.125$. On a given time slice an occupied state is denoted by a "1". (b) Typical configuration after several hundred Monte Carlo sweeps over the lattice.

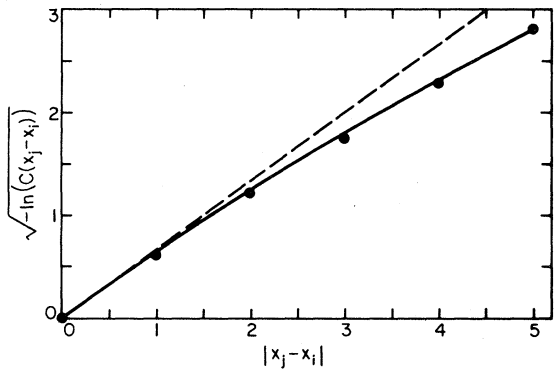

FIG. 5. Plot of the single-particle density-density correlation function vs distance at an imaginary-time separation $\tau=\beta/2$. Dashed line is the free-particle result, Eq. (3.4), whose slope $\sqrt{2m/\beta}$ is proportional to the particle mass. Solid line is the exact result for the tight-binding problem with $\epsilon_k=-2t\cos k$. Points give the Monte Carlo data with the rms errors the size of the points.

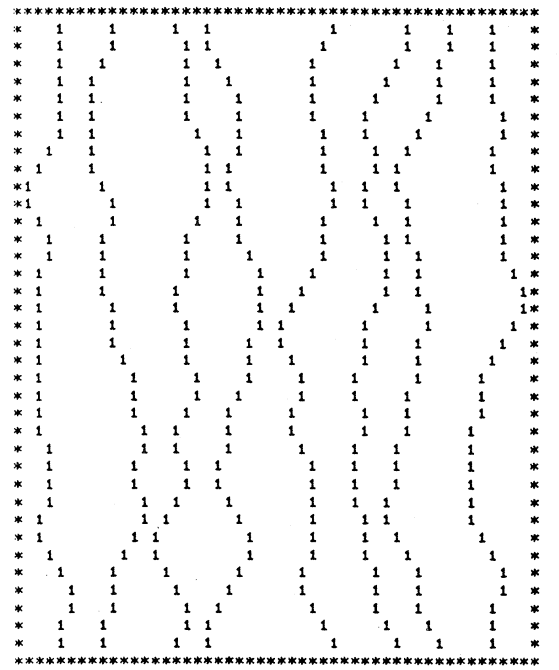

FIG. 6. Typical configuration of eight noninteracting fermions moving on a 48-site lattice and obeying the Pauli principle.

$V=2t$. Figure 7(a) shows a typical configuration for 24 electrons on 48 sites with $t=1$ and $V=0$. Here the only correlations are due to the Pauli principle. It is straightforward to calculate the internal energy for this system, and results for a 40-site system with 20 electrons are given in Table III. For comparison the exact $E(T)$ results for a *canonical ensemble* are also listed. The results labeled $E_{\rm CB}$ are "numerical" calculations for the checkerboard breakup. Clearly the checkerboard breakup provides an excellent approximation to the exact results, and the Monte Carlo calculation is working within its indicated rms error limits.

Figure 7(b) shows a configuration for $t=1$ and $V=3.0$. For this interaction strength, the charge-

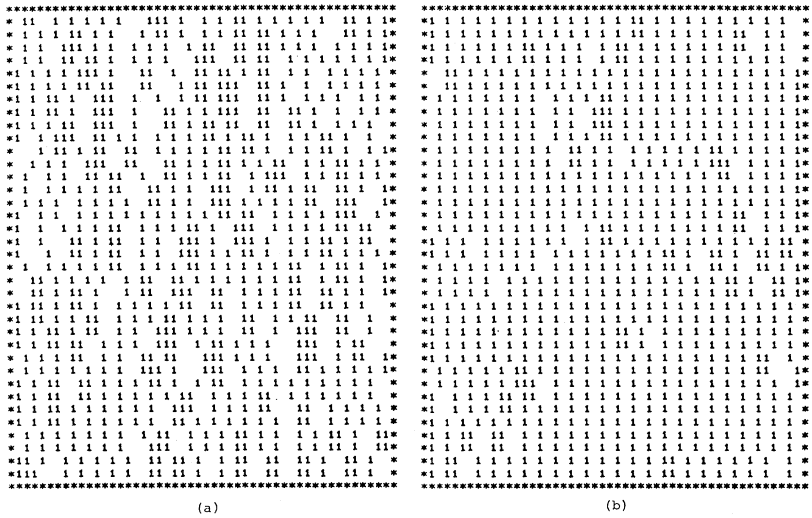

(a) (b)

FIG. 7. (a) Typical configuration for a half-filled band of 24 spinless fermions on a 48-site lattice with $V=0$. (b) Typical configuration for a half-filled band with $t=1$ and $V=3$. On a given time slice the fermions tend to occupy every other lattice site leading to a CDW state. The temperature is sufficiently low that the defects represent vacuum fluctuations rather than thermal ones.

TABLE III. Internal energy per site for 20 noninteracting electrons ($t=1, V=0$) on a 40-site periodic lattice at various temperatures. E (exact) and E_{CB} give results obtained from numerically evaluating the canonical and checkerboard partition functions, respectively. E_{MC} lists the Monte Carlo results obtained from 10 000 measurements, each separated by five lattice sweeps. For E_{CB} and E_{MC}, $\Delta\tau=0.1$.

T	E (exact)	E_{CB}	E_{MC}
0.5	−0.5659	−0.5668	−0.5668±0.0032
0.7692	−0.4810	−0.4818	−0.4845±0.0016
1.0	−0.4141	−0.4148	−0.4162±0.0030
1.25	−0.3548	−0.3554	−0.3565±0.0027
1.429	−0.3202	−0.3208	−0.3176±0.0026
1.667	−0.2824	−0.2828	−0.2824±0.0025
2.0	−0.2413	−0.2416	−0.2464±0.0023
2.5	−0.1971	−0.1975	−0.1979±0.0023

density-wave character of the state is clearly visible. Consider a given row and note that every other site tends to be occupied. There are, of course, defects. These are "vacuum fluctuations" since the temperature is too low to produce sizable thermal fluctuations. As discussed in Sec. II, an average over the time slices which can be crudely done by eye gives $|\langle n_1 \cdots n_N | \psi_0 \rangle|^2$. Naturally, as V approaches the critical point at $V=2t$, a large number of configurations must be averaged over to determine whether $|\psi_0\rangle$ is a normal or a charge-density-wave state.

The density-density correlation function

$$\rho(l)=\langle n_{i+l} n_i \rangle \tag{3.5}$$

is shown in Figs. 8(a)–8(c) for $\beta=4$, $t=1$, and $V=1.5$, 2.0, and 2.5 respectively. It is clear that this correlation function decays for $V=1.5$ and does not for $V=2.5$. Figure 9(a) shows the Fourier transform of the density-density correlation function

$$S(q)=\frac{1}{N}\sum_{i,l} e^{iql}(\langle n_{i+l} n_i \rangle - \langle n \rangle^2) \tag{3.6}$$

at low temperature ($\beta=4$). For the free case $V=0$, the structure factor has the property that $S(q)=0.5-S(\pi-q)$. As shown, the results are in excellent agreement with the exact results for a grand canonical ensemble shown as the solid line except at the points $q=0$ and $q=\pi$. At these two points, the fixed particle number of the canonical ensemble implies that the canonical structure factor takes the values $S(0)=0$ and $S(\pi)=0.5$. However, when the number of sites goes to infinity the canonical structure factor is equal to the grand canonical structure factor for $q\neq 0$ or π so that the canonical structure factor is discontinuous at $q=0$ and $q=\pi$ for finite temperatures. This effect can just be seen at $T=0.25$ for the 40-site lattice as shown by the fit of the Monte Carlo data to the ground canonical curve as $q\to 0$ and $q\to\pi$. Over most of the range of q, $S(q)$ is close to its zero-temperature value $q/2\pi$. One can show for $V=0$ that in an infinite system $S(q\to 0,T)=kT/\pi$.

For $V=2$, $S(q)$ develops a peak at $q=\pi$ signaling the tendency for formation of a charge-density wave, as shown in Fig. 9(b). At $V=2$, the fermion model can be mapped onto the isotropic antiferromagnetic Heisenberg chain where the corresponding S^z-S^z correlation function is expected to decay as $(-1)^l/l$.[14] This implies that $S(\pi)\sim \ln N$ where N is the number of sites of the system. In Fig. 9(c) we have plotted $S(\pi)$ vs $\ln N$ for N varying between 4 and 100. This clearly shows the expected $\ln N$ variation. Further discussion of this model is given in Sec. V.

It is also interesting to examine what happens when an additional fermion is added to a system in a charge-density-wave ground state. Hubbard[15] originally suggested that two entities, each with a charge of one-half, would form. Figure 10(a) shows the initial configuration with one added electron, and Fig. 10(b) a resulting typical configuration after warm up. Indeed, two entities are clearly visible. Just as in the free-particle case, one could obtain an effective mass for these entities by studying their motion in τ.

IV. THE EXTENDED HUBBARD MODEL

As we have seen, the spinless, half-filled, one-dimensional electron gas with near-neighbor Coulomb interaction can exhibit a normal or charge-density-wave ground state. When spin de-

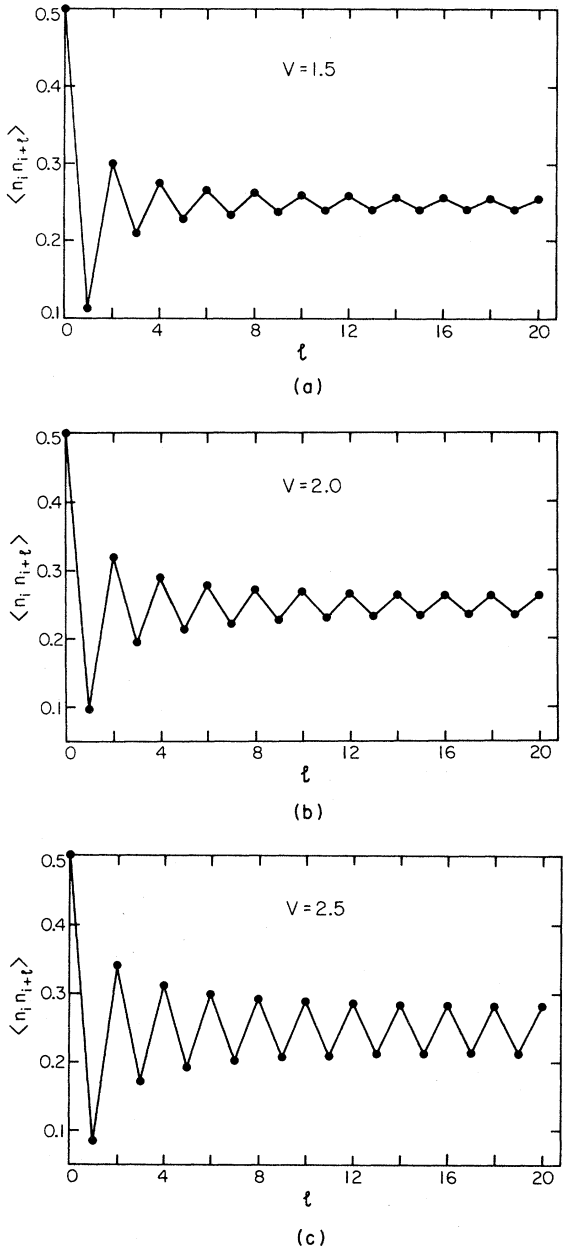

FIG. 8. Equal-time density-density correlation function vs site separation for a half-filled-band spinless-fermion model with (a) $V=1.5$, (b) 2.0, and (c) 2.5, respectively. Here $t=1$ and $\beta=4$.

grees of freedom are introduced, the allowed ground-state configurations become much richer including spin-density waves (SDW's) and singlet and triplet superconducting pairing, as well as the charge-density state. It is natural to introduce an on-site interaction

$$U \sum_i n_{i\uparrow} n_{i\downarrow} \tag{4.1}$$

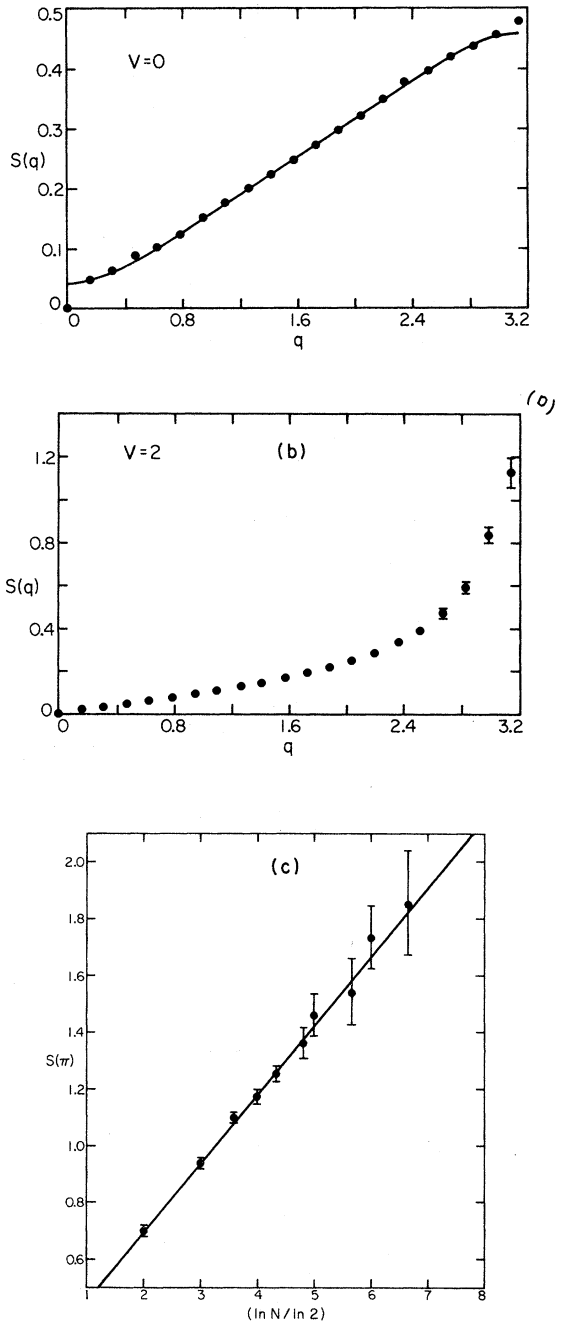

FIG. 9. (a) Points showing Monte Carlo data for the structure factor for a 40-site lattice containing 20 noninteracting electrons ($t=1, V=0$) at low temperature, $\beta=4$. Solid line is the grand canonical result for this system. (b) Monte Carlo results for the structure factor for $t=1$ and $V=2$ at $\beta=4$. Note the difference in scale between parts (a) and (b). (c) Structure factor $S(\pi)$ for momentum transfer $q=2p_F=\pi$ for the half-filled case with $V/2t=1$ vs the lattice size. Here $L=N$ and data from lattices with $N=4$ to 100 were computed. Data clearly show the $\ln N$ scaling dependence.

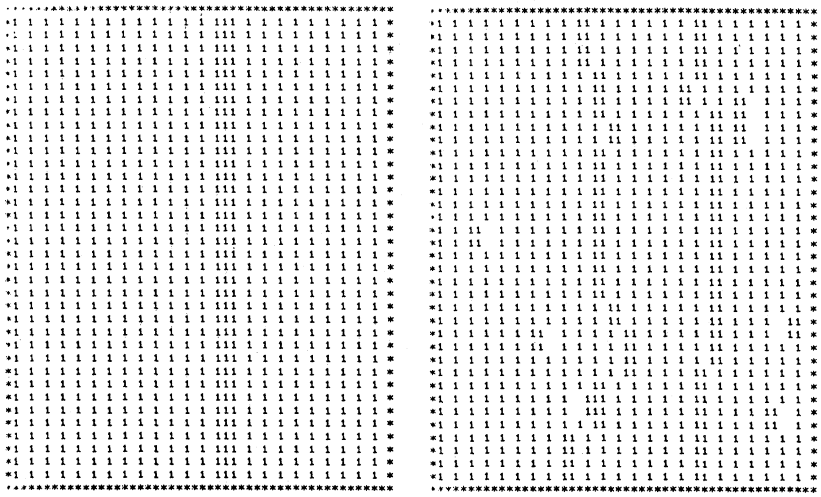

FIG. 10. (a) Initial configuration with one additional fermion added to a half-filled band ($t=1, V=4$). (b) Typical configuration after the system has warmed up showing two entities.

as well as the near-neighbor density-density interaction

$$V\sum_i n_{i+1}n_i \ . \tag{4.2}$$

Combined with the hopping (band) term,

$$-t\sum_{i,\sigma}(C^{\dagger}_{i+1,\sigma}C_{i,\sigma}+\text{H.c.}) \ , \tag{4.3}$$

this model is called the extended Hubbard model.[16] An approximate ground-state phase diagram obtained from weak-coupling renormalization-group (RNG) calculations[17] is sketched in Fig. 11. Clearly the rich behavior of this phase diagram offers an interesting test of the methods discussed here.

It is straightforward to treat electron spin by introducing two fermions fields $n_{\pm}(i,j)$ which give the occupation of spin-up or spin-down electrons on spatial site i and time slice j. Pictorially one can imagine two checkerboards, one laying above the other with the space-time paths of the spin-up electrons laid out on the upper board and those of the spin-down electrons laid out on the lower board. New paths are generated by making moves on either board of the type discussed for the spinless fermions in the previous sections. The change in the interaction

$$U\sum_i n_{i\uparrow}n_{i\downarrow}+V\sum n_i n_{i+1}$$

enters in the usual way in computing the ratio R which determines the probability of accepting a given move.

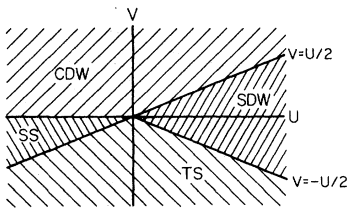

FIG. 11. Approximate ground-state phase diagram for the extended Hubbard model. (TS labels the triplet superconducting phase.)

Figure 12 shows a typical picture obtained for the free case in which $U=V=0$. Here we have taken 20 sites with 10 spin-up and 10 spin-down electrons. Occupied spin-up sites are denoted by $+$, spin-down sites, by $-$, double by $\#$, and those that are empty by a blank space. For the free case, the spin-up, $(+)$ electrons move independently of the spin-down $(-)$ electrons but each species naturally obeys the Pauli principle. The properties of the system are those of a normal one-dimensional free-electron gas with band energies $\epsilon_k=-2t\cos k$.

With $U>0$ and $V=0$ the ground state, according to the phase diagram of Fig. 11, should exhibit a spin-density-wave structure. Figure 13 shows a typical configuration for $U=6.0$. Here we measure energies in units of t, and a relatively large value of U has been selected so that a single configuration can provide a useful sample of the character of the ground state. As previously discussed, physical quantities are computed by averaging over many independent configurations. This not only gives the required ensemble average, but just as in a real ex-

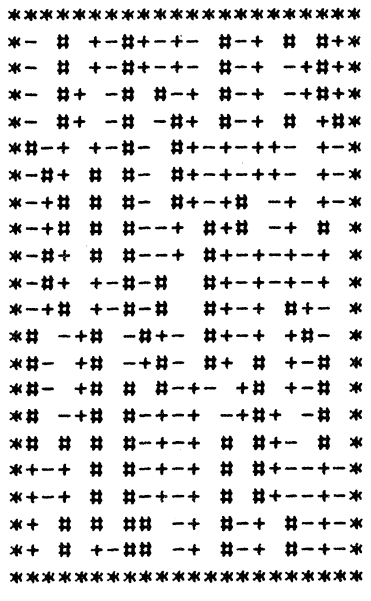

FIG. 12. Configuration of the electrons in an extended Hubbard model with $U=V=0$. Sites with a spin-up electron are denoted by $+$, a spin-down one by $-$, double occupation by #, and zero occupation by a blank space.

periment, fluctuations are averaged over, and the detailed correlations become visible. They are filtered out by the particular operators that one chooses to study. By taking U large, fluctuations are suppressed, and the correlations under discussion become visible by examining a single configuration.

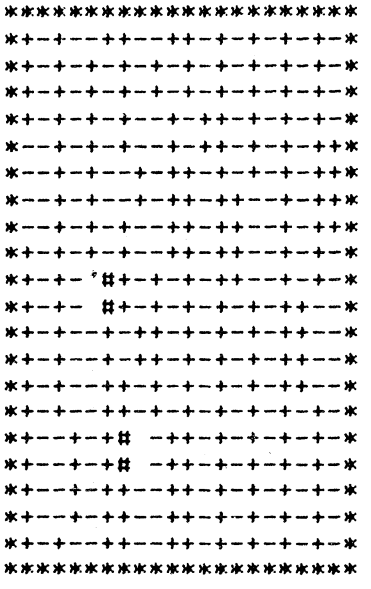

FIG. 13. Configuration for $U=6$ and $V=0$ showing spin-density-wave character.

In Fig. 13 note the regions of alternating spins which are characteristic of a spin-density-wave state. As before, the temperature is sufficiently low that the fluctuations giving rise to defects are vacuum fluctuations. A more precise characterization of the nature of the ground state can be obtained by evaluating the staggered spin-density-wave correlation function

$$\mathcal{C}_{\mathrm{SDW}}(l)=(-1)^l\langle S^z_{i+l}S^z_i\rangle\ , \tag{4.4}$$

with

$$S^z_i=\tfrac{1}{2}(n_{i\uparrow}-n_{i\downarrow})\ .$$

Here, as in all our calculations, the site i is averaged over. For the diagonal occupation-number expectation values we can, as discussed in Sec. II, also average over all time slices of a given configuration. Typically 5000 independent configurations were averaged over to obtain the results presented here. The staggered spin-density-wave correlation function $\mathcal{C}_{\mathrm{SDW}}$ is plotted in Fig. 14 and shows the expected algebraic decay associated with this phase. (For infinite U this model is equivalent to an isotropic Heisenberg antiferromagnetic chain where the spin density decays as l^{-1}.) For large positive values of U the charge-density-wave correlations as well as the pairing correlations are negligible.

An attractive effective electron-electron interaction may arise from lattice polarization or possibly electron polarization on molecules surrounding the chain. When $U<0$, there is a tendency for on-site pairing. If $V>0$, these pairs repel each other and, according to the phase diagram of Fig. 11, the system has a charge-density-wave ground state. A typical configuration for $U=-6$ and $V=0.4$ is illustrated in Fig. 15 and clearly shows the formation of a charge-density-wave state.

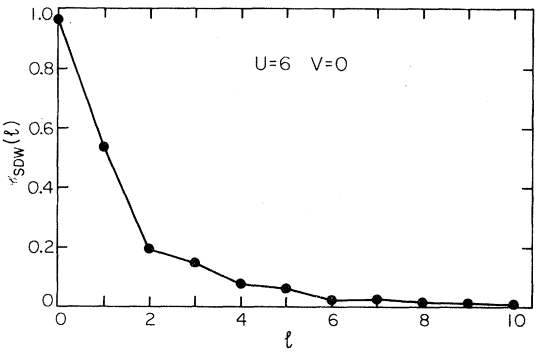

FIG. 14. Staggered spin-density-wave correlation function vs distance for $U=6$ and $V=0$.

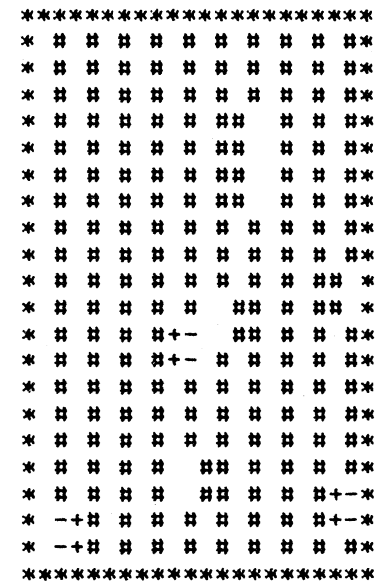

FIG. 15. Configuration for $U=-6$ and $V=0.4$ showing a charge-density-wave structure.

When both U and V are attractive there is a marked change in the appearance of the configurations. Figure 16 shows a configuration for $U=-6$ and $V=-0.4$. Clearly, on-site spatial pairing is predominant due to the large negative value of U. There is also a tendency for the pairs to cluster due to V being attractive. However, it remains a question as to whether the system should be characterized as superconducting. This is a question that is not so clearly evident in a position-space picture since superconductors are characterized by order in momentum space. The lack of position-space order evident for $V<0$ in Fig. 16 may reflect the existence of momentum-space ordering.

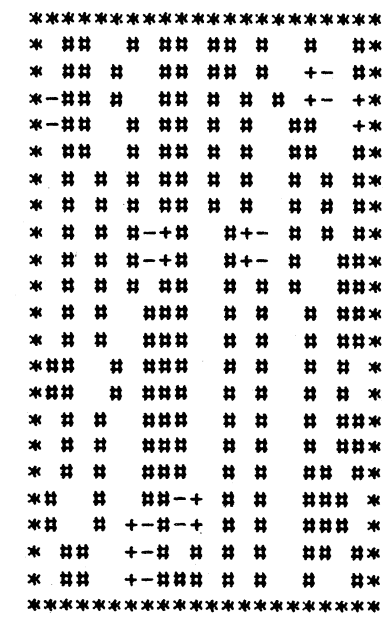

FIG. 16. Configuration for $U=-6$ and $V=-0.4$. This type of pattern is characteristic of single superconducting pairing.

To test for this type of order we need to calculate correlation functions. For U large and negative the spin-density-wave correlations are negligible. What are interesting to compute are the CDW correlations

$$\mathcal{C}_{\mathrm{CDW}}(l)=(-1)^l\langle n_{i+l}n_i\rangle \tag{4.5}$$

and the singlet superconducting (SS) correlations

$$\mathcal{C}_{\mathrm{SS}}(l)=\langle C_{i+l\uparrow}C_{i+l\downarrow}C_{i\uparrow}^{\dagger}C_{i\downarrow}^{\dagger}\rangle\ . \tag{4.6}$$

As usual we average over i for the periodic ring to improve statistics. However, as discussed in Sec. II, the evaluation of off-diagonal correlations such as Eq. (4.6) requires us to break the world lines at one time slice and evaluate the correlations along this slice.

The CDW correlation function Eq. (4.5) and the SS correlation function Eq. (4.6) are plotted for $V=-0.4$ and 0.4 in Figs. 17 and 18. For an attractive V, the singlet superconducting correlations dominate, while for a repulsive V the system is in a charge-density-wave state as was clear from the configuration shown in Fig. 15. In one dimension, the charge-density-wave ground state exhibits long-range order, while in the singlet superconducting state $\mathcal{C}_{\mathrm{SS}}(l)$ decays algebraically. In Fig. 19 the equal-time single-particle Green's function

$$G_{\sigma}(l)=\langle C_{i+l\sigma}C_{i\sigma}^{\dagger}\rangle \tag{4.7}$$

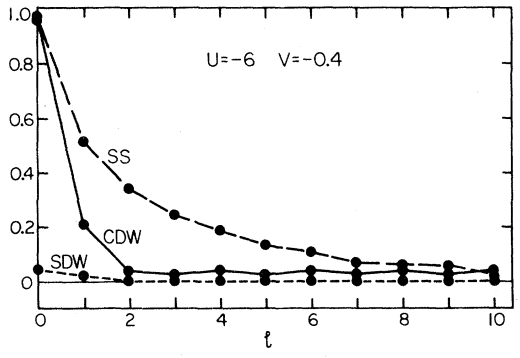

FIG. 17. Correlation functions for $U=-6$ and $V=-0.4$ showing that the singlet superconducting correlations dominate. The superconducting ground state of an infinite one-dimensional system is characterized by the algebraic decay of the singlet superconducting correlations.

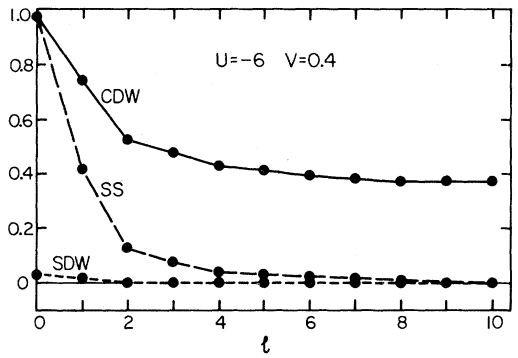

FIG. 18. Correlation functions for $U=-6$ and $V=0.4$ show that the system is in a CDW state. The CDW ground state of an infinite one-dimensional system has a broken symmetry and exhibits long-range order.

is compared with the singlet-pairing correlation function $\mathscr{C}_{SS}(l)$, the single-particle Green's function decays rapidly to 0 due to sign alterations. These are canceled by the opposite phases arising from the time reversed $-\sigma$ partner of the pair in the superconducting state leading to the much slower algebraic decay of $\mathscr{C}_{SS}$.

V. THE GROSS-NEVEU MODEL

The Gross-Neveu model[18] has been of interest in high-energy physics as an example of a system which exhibits both asymptotic freedom and spontaneous breaking of chiral symmetry.

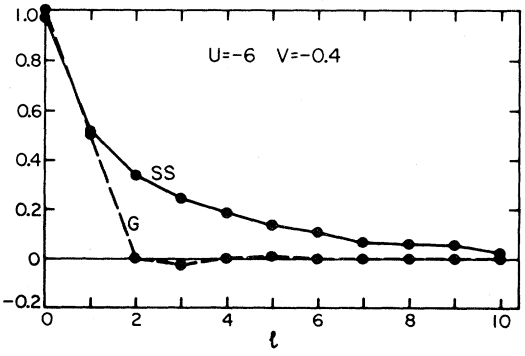

FIG. 19. Single-particle Green's function G decays rapidly to zero because of single-particle phase shifts. In the singlet superconducting correlation function $\mathscr{C}_{SS}$ these are canceled due to pairing of time-reversed states.

The continuum Hamiltonian for this model is

$$H=\int dx\left[\psi^{\alpha\dagger}(x)\sigma_x\frac{1}{i}\frac{\partial}{\partial x}\psi^{\alpha}(x)-\frac{g^2}{2N_f}[\psi^{\alpha\dagger}(x)\sigma_z\psi^{\alpha}(x)]^2\right]. \tag{5.1}$$

Here σ_x and σ_z are the usual Pauli spin matrices and $\alpha=1,\ldots,N_f$ is the internal-symmetry index. Summation over repeated indices is understood.

If we naively place the theory on a lattice by writing (j denoted the lattice site)

$$H=\sum_j\left[\frac{1}{2i}\psi_j^{\alpha\dagger}\sigma_x(\psi_{j+1}^{\alpha}-\psi_{j-1}^{\alpha})-\frac{g^2}{8N_f}(\psi_j^{\alpha\dagger}\sigma_z\psi_j^{\alpha}+\psi_{j+1}^{\alpha\dagger}\sigma_z\psi_{j+1}^{\alpha})^2\right], \tag{5.2}$$

then we encounter the well-known spectrum-doubling problem. To avoid it we follow Kogut and Susskind[19] and place the upper components of ψ^{α} on even lattice sites and the lower components on odd ones. That is, we write

$$\psi_j^{\alpha}=(-i)^j\begin{bmatrix}C_j^{\alpha}\\0\end{bmatrix},\ j\text{ even},\qquad \psi_j^{\alpha}=(-i)^j\begin{bmatrix}0\\C_j^{\alpha}\end{bmatrix},\ j\text{ odd}. \tag{5.3}$$

The Hamiltonian of Eq. (5.2) then becomes

$$H=\sum_j\left[-\tfrac{1}{2}(C_j^{\alpha\dagger}C_{j+1}^{\alpha}+C_{j+1}^{\alpha\dagger}C_j^{\alpha})-\frac{g^2}{8N_f}(C_j^{\alpha\dagger}C_j^{\alpha}-C_{j+1}^{\alpha\dagger}C_{j+1}^{\alpha})^2\right]. \tag{5.4}$$

The reason for averaging the interaction over two lattice sites in Eq. (5.2) should now be clear.[20]

The naive lattice Hamiltonian of Eq. (5.2) is invariant under translation by a single lattice site, $\psi_j^{\alpha}\rightarrow\psi_{j+1}^{\alpha}$ and under the chiral transformation $\psi_j^{\alpha}\rightarrow\sigma_x\psi_j^{\alpha}$. For the Susskind fermions translational invariance corresponds to invariance under translation by the two lattice sites, $C_j^{\alpha}\rightarrow C_{j+2}^{\alpha}$, while chiral invariance corresponds to invariance to translation by a single lattice site $C_j^{\alpha}\rightarrow C_{j+1}^{\alpha}$. The order parameter that measures the spontaneous breaking of chiral symmetry is $\psi_j^{\alpha\dagger}\sigma_x\psi_j^{\alpha}$ for naive fermions and

$$Q_5^\alpha = N^{-1/2} \sum_j (-1)^j C_j^{\alpha\dagger} C_j^\alpha \tag{5.5}$$

for the Susskind fermions. There is no summation over α in Eq. (5.5).

If we work on a lattice with N sites and use periodic boundary conditions for the ψ_j^α, then with our choice of phases the C_j^α satisfy periodic or antiperiodic boundary conditions depending on whether or not N is a multiple of four. (N must be even.) However, because we neglect fermion configurations with nonzero winding numbers, there is no difference between these boundary conditions in our Monte Carlo algorithm.

Notice that for one fermion flavor, $N_f=1$, the Gross-Neveu model is identical to the spinless fermion model defined in Eq. (1.2) with $t=\frac{1}{2}$ and $V=g^2/4$. For $N_f=2$ the Gross-Neveu model is the extended Hubbard model with $t=\frac{1}{2}$ and $V=-U/2=g^2/8$.

We focus our attention on the correlation function

$$G(\tau)=\frac{1}{N_f}\sum_{\alpha=1}^{N_f}\langle Q_5^\alpha(\tau)Q_5^\alpha(0)\rangle \tag{5.6}$$

and the order parameter

$$M=\langle Q_5^\alpha\rangle N^{-1/2}\,|_{N\to\infty}\ . \tag{5.7}$$

Considerable information can be obtained by studying $G(\tau)$ as a function of the number of lattice sites, N. When chiral symmetry is spontaneously broken so that $M\neq 0$, $G(\tau)\to_{N\to\infty} NM^2$. We expect this to be the case for all values of g^2 when $N_f\geq 2$ and for $g^2>4$ when $N_f=1$. For $N_f=1$ and $g^2<4$, $M=0$ and $G(\tau)$ approaches a finite limit as $N\to\infty$. Exactly at the critical point $G(0)$ grows like $\ln N$ as we have already noted. We illustrate these points in Figs. 20 and 21 by plotting $G(0)$ and $G(\beta/2)$ vs g^2/N_f on different sizes of lattices for $N_f=1$ and 2. In each case β^{-1} is much smaller than the other energy scales in the problem. Notice that at the phase transition point the variation in $G(0)$ with $\ln N$ is visible as is illustrated more fully in Fig. 9.

We extract the order parameter, M, by fitting $G(\tau)$ to the form

$$G(\tau)=NM^2+\delta_{N_f,1}\ln NC(\tau)+g(\tau)\ . \tag{5.8}$$

Results are shown in Fig. 22. We have made the fit for $\tau=0$ and $\beta/2$ and obtained identical results within statistical errors. For $N_f=1$, $C(\beta/2)=0$ for all g^2 as expected. We find that $C(0)$ differs from zero in that range of g^2 for which the correlation length is larger than or of the order of the lattice size, also as expected.

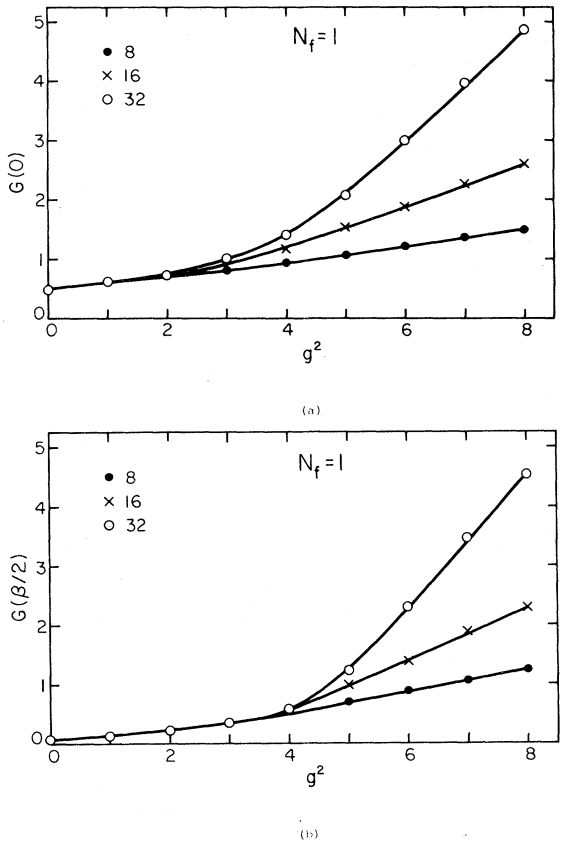

FIG. 20. (a) Correlation function $G(0)$ defined in Eq. (5.6) for $N_F=1$. We show results for lattices with 8 sites (solid circles), 16 sites (crosses), and 32 sites (empty circles). Statistical errors are within the symbols in all cases. (b) Correlation function $G(\beta/2)$ for $N_F=1$. We show results for lattices with 8 sites (solid circles), 16 sites (crosses), and 32 sites (empty circles). Statistical errors are within the symbols. As expected, $G(\beta/2)$ is independent of lattice size for $g^2\leq 4$.

In principle one can calculate the gap from the τ dependence of $G(\tau)$. In practice this is difficult because of finite-size effects. To take the finite-size effects into account we fit $G(\tau)$ with the correlation function from free-field theory on an identical lattice. The single (mass) parameter in the free-field-theory correlation function is determined by requiring that it agrees with our Monte Carlo results at $\tau=\beta/2$. The gap and the order parameter are then both determined, and the results for the order parameter agree with those obtained from Eq. (5.8). A typical fit to the correlation function is shown in Table IV. The fact that the correlation function is well fit by free-field theory for all values of τ rather

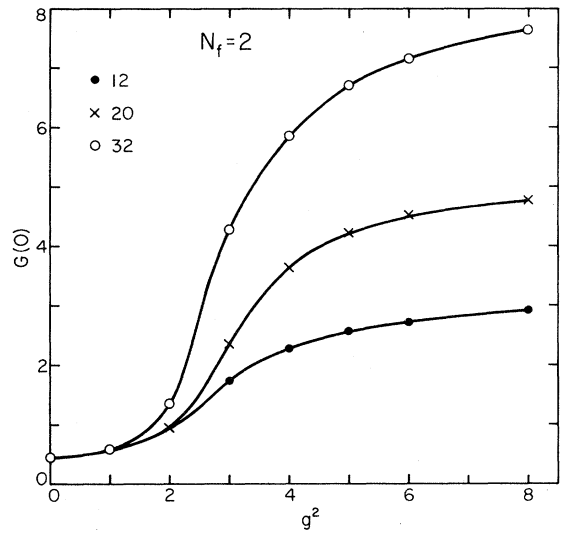

FIG. 21. Correlation function $G(0)$ for $N_F=2$. We show results for lattices with 12 sites (solid circles), 20 sites (crosses) and 32 sites (empty circles). Statistical errors are within the symbols. Size dependences of $G(0)$ are evident for $g^2>1$. For $g^2=1$ the correlation length is larger than the length of even the 32-site lattice.

than simply for large values of τ indicates that mean-field theory is valid. This appears to be the case for $N_f \geq 2$ for all but the smallest values of the coupling constant. In Fig. 23 we plot the gap versus g^2 for $N_f=10$. We also include the mean-field theory and asymptotic freedom predictions. More detailed results on this model will be given elsewhere.

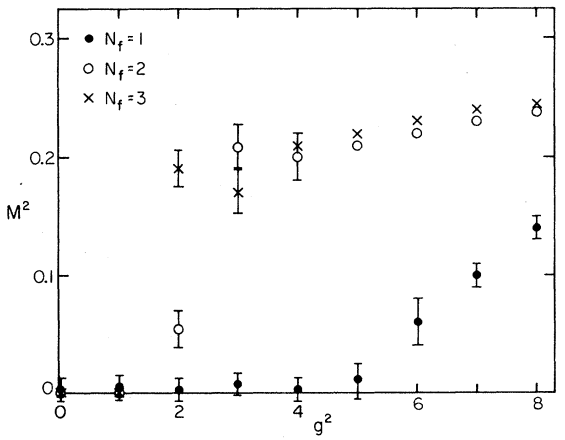

FIG. 22. M^2 as a function of g^2 for $N_F=1$ (dark circles), $N_F=2$ (crosses), and $N_F=3$ (empty circles). Where no error bars are shown, the errors lie within the symbols.

TABLE IV. Gross-Neveu model correlation function defined in Eq. (3.6) for $N_F=10$ and $g^2=2$. G_{MC} is the Monte Carlo result and G_F is the one-parameter fit based on mean-field theory for the finite lattice.

τ	$G_{MC}(\tau)$	$G_F(\tau)$
0.0	1.937±0.005	1.934
0.5	1.803±0.005	1.800
1.0	1.757±0.006	1.756
1.5	1.741±0.006	1.741
2.0	1.736±0.006	1.735
2.5	1.734±0.006	1.734
3.0	1.733±0.006	1.733
3.5	1.733±0.006	1.733
4.0	1.733±0.006	1.733

VI. AN ELECTRON-PHONON MODEL

In this section we consider the electron-phonon system, Eq. (1.3), as an example of a coupled fermion-boson system. The specification of the path integral now involves the fermion field $n_{\pm}(i,j)$ and the boson field $x(i,j)$. Just as before, i is a site index and j denotes a given time slice. The time grids $\Delta\tau_F$ and $\Delta\tau_B$ for the fermion and boson fields can be different and should be set so that $\Delta\tau_F t \ll 1$ and $\Delta\tau_B \Omega \ll 1$ with $\Omega=\sqrt{K/M}$. For example, if the phonons respond on a slow time scale so that $\Omega \ll t$, it is natural to have $\Delta\tau_B \gg \Delta\tau_F$ so that the phonon field remains the same for a number of fermion time slices. For the cases discussed here the time scales were taken to be roughly similar and the boson field was changed on every other fermion time line corresponding to multiples of the basic $\Delta\tau$ unit.

The procedure for updating the fermion field was

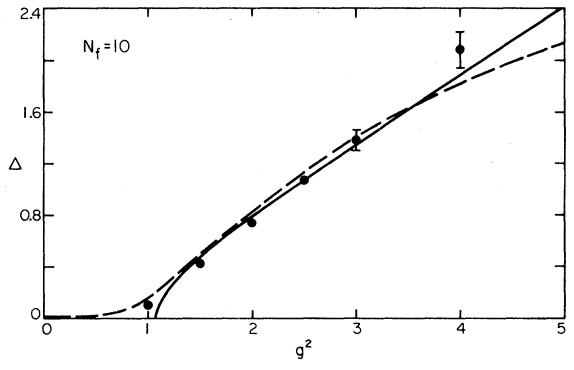

FIG. 23. Gap vs g^2 for the Gross-Neveu model with ten flavors. Dashed line is the asymptotic freedom prediction and solid line the mean-field-theory prediction for a finite lattice.

the same as previously discussed. For the bosons the Metropolis method was used. The boson field at a site would be shifted by a random amount Δr, with r a random number between $(-1,1)$ and Δ a set value. If the exponential of minus the change in action produced by this change in the boson field exceeded a random number between (0,1), the new value of the field was accepted. This could be repeated n times. Values of n and Δ were selected to optimize convergence. Typically n was set of order 5 and Δ was taken to be of order $(\Omega/K)^{1/2}$.

Before turning to the many-electron problem it is interesting to examine the one-electron problem.[6] For a system with $t=2.0$, $K=0.5$, $M=2.0$, and $\lambda=1.0$, a typical electron trajectory looks a great deal like that shown in Fig. 4(b). However, a careful examination shows that the spread in width of the trajectory appears narrower corresponding to a larger effective mass. A printout of the boson field shows a rough channellike region in which the molecules are contracted along the electron path.

In order to obtain a clearer picture of this phenomena, it is useful to consider the result of a *gedanken* experiment in which the lattice distortion is measured as a function of distance away from the electron:

$$C(l)=\sum_i \langle n_i x_{i+l} \rangle \ . \tag{6.1}$$

Here n_i is unity if the electron is at the ith site so that $C(l)$ measures the lattice distortion a distance l away from the instantaneous position of the electron. The correlation function $C(l)$, plotted in Fig. 24, clearly shows the lattice distortion surrounding the electron. In the adiabatic limit when $t \gg \Omega$, the size of the polaron is approximately given by t/ω_B with $\omega_B=\lambda^2/2K$. This is equal to 2 in our case in rough agreement with Fig. 24 although the parameters are not really into the adiabatic region $(\Omega=\sqrt{K/m}=0.5)$. The effective mass can be determined by calculating

$$\langle n(i+l,\beta/2)n(i,0)\rangle$$

as discussed in Sec. III for the case of a free particle. Figure 25 shows a plot of

$$\left[-\ln\left[\frac{\langle n(i+l,\beta/2)n(i,0)\rangle}{\langle n(i+l,0)n(i,0)\rangle}\right]\right]^{1/2}$$

vs l similar to that shown in Fig. 5 for the noninteracting case. The open circles correspond to the noninteracting case with $t=2.0$ and $\lambda=0.0$. In this case the effective mass $m^*=(2t)^{-1}$. The solid circles are for the interacting case with $t=2.0$, $K=0.5$, $M=2.0$, and $\lambda=1.0$. The effective mass has clearly increased. The solid line passes through points corresponding to a noninteracting system with $t=\frac{2}{3}$ and implies an enhancement of the effective mass by a factor of $\frac{3}{2}$. The adiabatic theory of the large polaron gives an enhancement of $(\frac{8}{15})(\omega_B/\Omega)^2 \simeq 2$ for these parameters.

By increasing the fermion occupation number it is possible to study a variety of problems ranging from a dilute polaron gas to the case of a half-filled band. In Fig. 26(a) typical fermion and boson configurations for the case of a half-filled band of spin-up and -down electrons in a strong coupling case with $t=1$, $\Omega=0.5$, and $\lambda=0.75$ are shown. From the fermion trajectories it is clear that the system is in a charge-density-wave state. The phonon-field configuration in Fig. 26(b) is characterized by writing a + sign for a positive value of

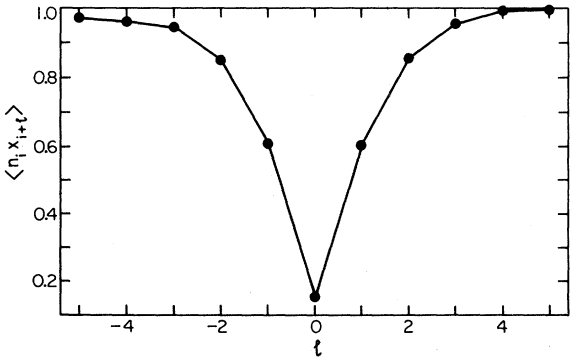

FIG. 24. Average lattice distortion $C(l)=\langle M_i x_{i+l} \rangle$ surrounding an electron vs l.

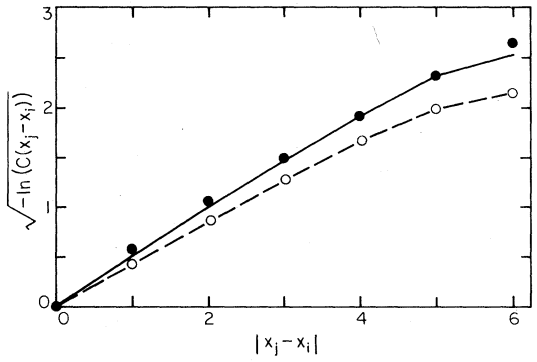

FIG. 25. Electron density-density correlation function vs distance at an imaginary-time separation $\tau=\beta/2$. Open points are for a noninteracting system ($\lambda=0$) with $t=2.0$. Solid points are for the interacting system with $t=2.0$, $K=0.5$, $M=2.0$, and $\lambda=1.0$. For comparison, the solid line runs through a set of points obtained for a noninteracting system with $t=\frac{2}{3}$.

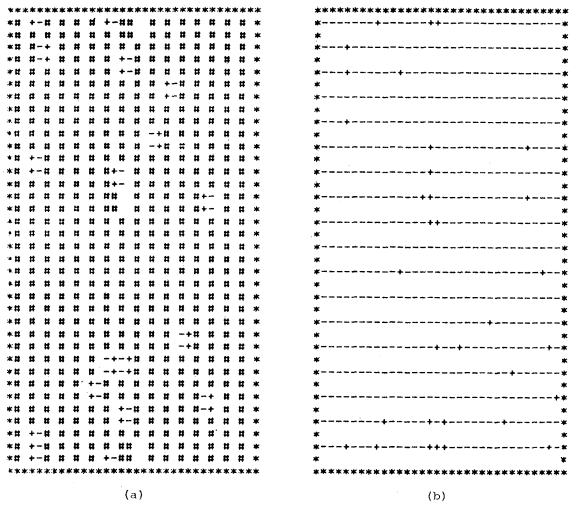

FIG. 26 (a) Typical electron configuration for $t=1$, $\Omega=0.5$, and $\lambda=0.75$. (b) Sign of the staggered field $(-1)^l x_l$ for the associated-lattice—Monte Carlo lattice configuration. System is clearly in a Peierls state in which the electrons exhibit a CDW and the lattice is dimerized.

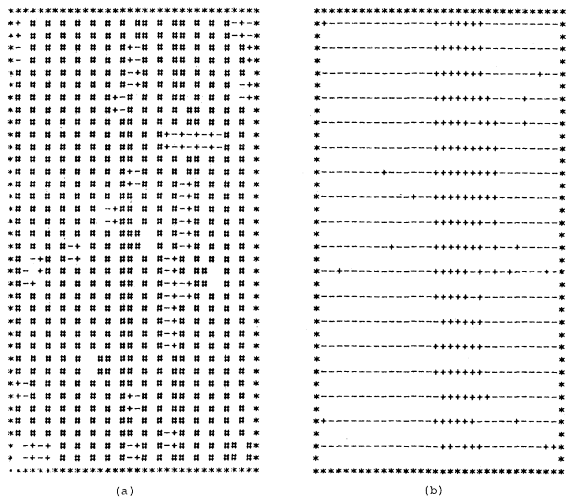

FIG. 27. Typical electron and lattice configurations for the case in which two electrons have been added to the previous configuration shown in Fig. 26. Examination of the electron configuration (a) near the regions where the staggered field changes sign shows the excess charges but note that the electrons are dominantly paired so the effective spin of the solitons is zero. Existence of two solitons is clearly evident in the staggered field of the lattice (b).

the *staggered* field $(-1)^l x_l$ and a $-$ sign for a negative value. With these parameters the system is clearly dimerized. This is just the well-known Peierls distortion.[7]

If we add a pair of electrons of opposite spin to the system shown in Fig. 26 and let it evolve for a few hundred Monte Carlo sweeps, we obtain typical configurations as shown in Fig. 27. In the electron configuration one sees two objects that evolve in time similar to the fractional charges in Fig. 10. Note that each of these objects must have a charge of 1, since we added two electrons to the system. However, unlike individual electrons, these objects do not carry spin, since it is clear from Fig. 27(a) that electrons are paired almost all of the time. Thus, they will not contribute to the magnetic susceptibility. These are the charged solitons (charge 1 and spin 0) discussed by Su, Schrieffer, and Heeger.[21] The lattice configuration [Fig. 27(b)] shows clearly the existence of two solitons and the tunneling from one dimerized ground state to the other (remember we are plotting the *staggered* field). Thus, our Monte Carlo simulation is in agreement with the Su-Schrieffer-Heeger[21] picture that doping occurs through the formation of charged solitons and not through semiconductor-band doping in these systems.

For the case of spinless electrons, as previously suggested[22] and more recently studied in detail using the present method,[23] the Peierls state can be destroyed by zero-point fluctuations of the lattice when Ω/t exceeds a critical value. As an example, Fig. 28 shows the lattice staggered correlation function

$$D(l)=(-1)^l\langle x_i x_{i+l}\rangle$$

for $t=1.0$, $\lambda=0.9$, and two different values of the ion mass M ($M=1.5$ and 0.2, with $K=0.25$) for the spinless case. For $M=1.5$ there is clearly long-range order, reduced by about 15% from the

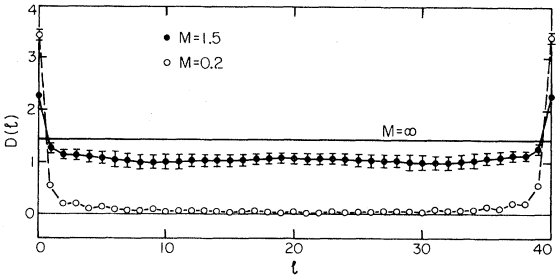

FIG. 28. Lattice-staggered correlation function $D(l)=(-1)^l\langle x_i x_{i+l}\rangle$ for $t=1.0$, $\lambda=0.9$, and two different values of the ion mass M. For an infinite chain there is a critical value of M below which the Peierls dimerization of the ground state is destroyed by the zero-point fluctuations of the lattice. Note the much larger zero-point fluctuations on site ($l=0,40$) for the smaller ion mass.

static limit results $M=\infty$, while for $M=0.2$ the long-range order has disappeared due to the quantum fluctuations. The Su-Schrieffer-Heeger model with interatomic lattice distortions has also been treated with this method.[23]

VII. CONCLUSIONS

The method presented in this paper offers the possibility of studying almost arbitrarily complicated one-dimensional (1D) interacting many-body systems. As discussed in the Introduction, it can be used qualitatively or quantitatively. It also complements other techniques allowing one to explore and extend them in a variety of ways. For example, there have been a number of studies based on finite-cell diagonalization. Our method gives the possibility of studying much larger systems. For instance, even for the 1D Hubbard model it becomes very difficult to diagonalize exactly systems bigger than eight sites. For systems with a larger number of degrees of freedom per site, such as the Anderson model, the number of sites for which one can perform exact diagonalization is much smaller. Perhaps more importantly, for systems with an infinite number of states per site like electron-phonon systems, finite-cell techniques are not applicable at all. Our method can easily handle systems of as many as 100 sites in all these cases. Naturally, there are statistical errors which are not present in the exact diagonalization for the small systems. However, knowing the exact results for small systems, one can match on to these to some desired accuracy using our Monte Carlo procedure and can then extend them to larger systems in a controlled manner. An example of this is the spinless-fermion problem.

For certain problems, the Bethe-*ansatz* provides exact solutions for the ground-state wave function and energy as well as excited-state energies of the infinite system. However, as is well known, it is difficult to obtain results for correlation functions and finite-temperature thermodynamic properties using Bethe-*ansatz* techniques. With our technique, however, we can directly calculate correlation functions. Furthermore, the calculations become simpler as the temperature is increased since fewer time slices are involved. Also, the modification or addition of interactions which move the problem outside the domain of the Bethe-*ansatz* approach can be directly dealt with.

An important result obtained from perturbative renormalization-group calculations for models of a 1D electron gas are scaling relations[24] ("*g*-ology") which provide, in principle, a means of scaling the original problem onto another whose properties may be known. The results for the Tomonaga model[25] and the Luther-Emery[26] backscattering problem are often used. Our method offers the possibility of going beyond the perturbative scaling regime to explore the entire parameter space. It allows us to treat retarded interactions that arise from electron-phonon or exitonic mechanisms. It also provides detailed information on short-range as well as long-range correlations. Working in the site representation on a lattice, umklapp processes enter in a natural way, and there are no delicate cutoff problems. Furthermore, the basic parameters which enter the Hamiltonian have a simple physical interpretation from a molecular point of view.

For the extraction of critical properties it will be of interest to combine our Monte Carlo technique with renormalization-group procedures. One related approach is finite-size scaling. This procedure has been used successfully for the spinless-fermion model, the extended Hubbard model, and the Gross-Neveau model.

Finally, compared with other Monte Carlo techniques for 1D systems, our method appears to be superior. All techniques that use the evaluation of a fermion determinant involve a computation time that goes up much faster than the size of the system, unlike our method. In addition, most of the "determinant techniques" become slow when the correlation length becomes large, i.e., when one approaches the free-fermion case. In contrast, with our method the equilibration time is about the same for the free case as for a case where there is a gap in the spectrum. Unlike other breakup techniques that have been used,[12] our method allows one to easily study an arbitrary number of time slices and, most importantly, does not involve minus-sign problems in one dimension.

As mentioned earlier, it is possible to utilize this general approach even if H is split according to quite different criteria. For example, a breakup into left and right movers has been carried out by Dahl.[27] This is not only exact in principle for the free case, but can be extended to handle long-range derivatives [such as the (SLAC) derivative]. It will be very interesting to study the effect of these different eigenspectra in certain relativistic models.

The most important outstanding question is the possibility of extending our method to higher dimensions. The formalism described can in principle be applied to higher-dimensional systems in the

same way. Consider for definiteness a two-dimensional (2D) square lattice. The Hamiltonian can again be broken up as $H=H_1+H_2$, with H_1 and H_2 composed of sums of Hamiltonians of nonoverlapping elementary squares. The building blocks for the space-time lattice are now elementary cubes, schematically illustrated in Fig. 29, and it is straightforward to compute all necessary matrix elements. Unfortunately, the product of all the matrix elements can now become negative for certain fermion configurations. These correspond for example to cases where two fermions interchange their positions at time slices 0 and β, and the world lines *do not* cross inside of an elementary block (this situation can clearly not arise in one dimension). In principle,[28] one can still write for the average of an operator 0,

$$\langle 0\rangle=\mathrm{tr}(OP)=\frac{\mathrm{tr}(O\,\mathrm{sgn}P\,|P|)}{\mathrm{tr}(\mathrm{sgn}P\,|P|)}$$

$$\equiv\frac{\langle O\,\mathrm{sgn}P\rangle_{|P|}}{\langle \mathrm{sgn}P\rangle_{|P|}}\ . \tag{7.1}$$

Here, P denotes the matrix elements divided by the partition function. One can then perform a Monte Carlo simulation using $|P|$ as the probability of the state and compute separately the numerator and denominator of Eq. (7.1). It should be pointed out that *no nonlocality* occurs in this algorithm as one could have expected, so that the computer time per sweep required for a quantum problem on a 2D space lattice is comparable to a three-dimensional (3D) Ising model. However, it is easy to convince oneself that both numerator and denominator in Eq. (7.1) go exponentially to zero with the size of the system at low temperatures. We have performed numerical simulations for 2D free-fermion systems and have found that statistical fluctuations make the evaluation of the quantities in Eq. (7.1) impossible except for cases where the band is almost empty or temperatures are rather high. Thus, it remains an open question whether some modification of this technique can be applied to higher-dimensional fermion problems. However, our formalism is directly applicable to certain high-dimensional quantum spin systems like the anisotropic Heisenberg model. We believe the method can handle the ferromagnetic and antiferromagnetic cases but is probably not applicable for systems with frustration due again to minus-sign problems. In addition, single-electron problems like the polaron for higher dimensions are directly amenable to treatment.

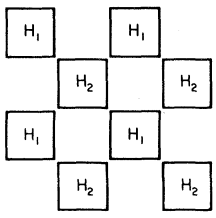

FIG. 29. Schematic top view of the cubes that make up the three-dimensional (x,y,τ) space. Here we are looking down the τ axis. The H_1 cubes occupy one $\Delta\tau/2$ time slice and the H_2 cubes occupy the next $\Delta\tau/2$ time slice, etc.

Returning to 1D systems, there exists a large number of organic charge-transfer compounds whose properties at not too low temperatures can presumably be modeled accurately by 1D Hamiltonians. Also, the effect of three-dimensionality at low temperatures can be taken into account approximately by using a self-consistent mean-field approximation for the interchain interactions.[29] It is straightforward within our method to include such mean-field terms in the Hamiltonian. We can, of course, also simulate the full behavior of an array of interacting chains, as long as no electron tunneling between chains is allowed.

With our formalism it is simple to compute static q-dependent correlation functions. It is also straightforward to compute τ-displaced correlation functions:

$$\chi(\tau)=\langle A(\tau)A(0)\rangle\ . \tag{7.2}$$

However, τ is an imaginary time. From an experimental point of view, it would be of interest to obtain correlation functions in *real* time or frequency. One cannot, of course, analytically continue numerical data. However, there exist various Padé approximant methods for obtaining the correlation functions at real frequencies from a knowledge of their analytic properties and their numerical values at a finite number of discrete imaginary points. It is however not clear how sensitive the results would be to statistical fluctuations in the Monte Carlo data and this problem needs further study. Fortunately, it is simple to compute the *zero-frequency* susceptibility,

$$\chi_{AB}(\omega=0)=\int_0^\beta d\tau\langle A(\tau)B(0)\rangle\ , \tag{7.3}$$

which measures the response of A to an external

field that couples linearly to the operator B. Work is in progress to study properties of various quasi-1D organic charge-transfer compounds using these techniques.

We have given only a brief description of the results from an application of our approach to relativistic models in one space dimension. A full description will be given elsewhere of the Gross-Neveau model, the Schwinger model, and possible extensions to models with higher-gauge symmetries.

ACKNOWLEDGMENTS

One of us (R.L.S.) would like to express his thanks for the hospitality extended to him at SLAC during the course of this work. This work was supported in part by National Science Foundation Grants Nos. PHY77-27084, PHY80-18938, and DMR80-01492, and in part by the U. S. Department of Energy under Contract No. De-AC03-76SF00515.

[1]R. P. Feynman and A. R. Hibbs, *Quantum Mechanics and Path Integrals* (McGraw-Hill, New York, 1965).

[2]M. Creutz and B. Freedman, Ann. Phys. 132, 427 (1981).

[3]F. Fucito, E. Marinari, G. Parisi, and C. Rebbi, Nucl. Phys. B 180, 369 (1981); D. J. Scalapino and R. L. Sugar, Phys. Rev. Lett. 46, 519 (1981); D. Weingarten and D. Petcher, Phys. Lett. 49B, 333 (1981); R. Blankenbecler, D. J. Scalapino, and R. L. Sugar, Phys. Rev. D 2278 (1981); A. Duncan and M. Furman, Nucl. Phys. B 140, 767 (1981); J. Kuti, Phys. Rev. Lett. 49, 183 (1982).

[4]J. Hirsch, D. J. Scalapino, R. L. Sugar, and R. Blankenbecler, Phys. Rev. Lett. 47, 1628 (1981).

[5]The techniques described in Ref. 4 have recently been used to study the Schwinger model. D. Martin and S. Otto (unpublished).

[6]T. Holstein, Ann. Phys. 8, 325 (1959).

[7]R. E. Peierls, *Quantum Theory of Solids* (Oxford University Press, London, 1955), p. 108.

[8]L. S. Schulman, *Techniques and Applications of Path Integration* (Wiley, New York, 1981).

[9]It is straightforward to extend this to $O((\Delta\tau)^3)$ by writing

$$e^{-\Delta\tau H}=e^{-\Delta\tau H_1/2}e^{-\Delta\tau H_2}e^{-\Delta\tau H/2}[1+O(\Delta\tau^3)]\ .$$

Because of the properties of the trace, this yields the same expression for Z as Eq. (2.4). It leads to slight modifications for expectation values, and we have not chosen to pursue it here, but rather have simply taken $\Delta\tau$ sufficiently small that the errors arising from Eq. (2.3) are less than or of order of the statistical errors associated with the Monte Carlo runs.

[10]M. Suzuki, S. Miyashita, and A. Kuroda, Prog. Theor. Phys. 58, 1377 (1977).

[11]This breakup was used to study the classical equivalence of 1D quantum systems by M. Barma and B. S. Shastry, Phys. Rev. B 18, 3351 (1978). We thank S. Chakravarty for bringing this reference to our attention.

[12]Other breakups are possible. See, for example, M. Suzuki, Prog. Theor. Phys. 56, 1454 (1976); H. De Raedt and A. Lagendijk, Phys. Rev. Lett. 46, 77 (1981).

[13]An interesting exception is the diamagnetic susceptibility of a ring. This is a small effect and will not be treated here.

[14]A. Luther and I. Peschel, Phys. Rev. B 12, 3908 (1975).

[15]J. Hubbard, Phys. Rev. B 17, 494 (1978).

[16]J. Hubbard, Proc. R. Soc. London Ser. A 276, 238 (1963).

[17]V. J. Emery, in *Highly Conducting One-Dimensional Solids*, edited by J. Devreese, R. Evrard, and V. van Doren (Plenum, New York, 1979).

[18]D. Gross and A. Neveu, Phys. Rev. D 10, 3235 (1974).

[19]J. Kogut and L. Susskind, Phys. Rev. D 11, 395 (1975); T. Banks, L. Susskind, and J. Kogut, *ibid.* 13, 1043 (1975).

[20]Monte Carlo calculations of the Gross-Neveu model with spectrum doubling have been made by Y. Coher, S. Elitzur, and E. Rabinovici, Phys. Lett. 104B, 289 (1981). They do not average the interaction over neighboring lattice sites. As a result, in their model chiral symmetry is not broken at large values of the coupling. However, for weak coupling they do find chiral-symmetry breaking and the behavior predicted by asymptotic freedom. Our formulation is identical to that of A. Zee, Phys. Rev. D 12, 3251 (1975) and J. Shigmitsu and S. Elitzur, *ibid.* 14, 1988 (1976).

[21]W. P. Su, J. R. Schrieffer, and A. J. Heeger, Phys. Rev. B 22, 2099 (1980).

[22]D. J. Scalapino and R. L. Sugar, Phys. Rev. B 24, 4295 (1981).

[23]J. E. Hirsch and E. Fradkin (unpublished).

[24]N. Menyhard and J. Solyom, J. Low Temp. Phys. 12, 529 (1973).

[25]S. Tomonaga, Prog. Theor. Phys. 5, 349 (1950).

[26]A. Luther and V. J. Emery, Phys. Rev. Lett. 33, 589 (1974).

[27]D. Dahl (unpublished).

[28]This approach was used by H. DeRaedt and A. Lagendijk (see Ref. 12).

[29]D. J. Scalapino, Y. Imry, and P. Pincus, Phys. Rev. B 11, 2042 (1975).